Utilization of Supercapacitors in Adaptive Protection Applications for Resiliency against Communication Failures: A Size and Cost Optimization Case Study

Hany F. Habib, Mohamad El Hariri, *Student Members IEEE,* Ahmed Elsayed, *member, IEEE* and Osama A. Mohammed, *Fellow IEEE*

***Abstract*— Microgrids' adaptive protection techniques rely on communication signals from the point of common coupling to adjust the corresponding relays' settings for either grid-connected or islanded modes of operation. However, during communication outages or in the event of a cyberattack, relays settings are not changed. Thus adaptive protection schemes are rendered unsuccessful. Due to their fast response, supercapacitors, which are present in the microgrid to feed pulse loads, could also be utilized to enhance the resiliency of adaptive protection schemes to communication outages. Proper sizing of the supercapacitors is therefore important in order to maintain a stable system operation and also regulate the protection scheme's cost. This paper presents a two-level optimization scheme for minimizing the supercapacitor size along with optimizing its controllers' parameters. The latter will lead to a reduction of the supercapacitor fault current contribution and an increase in that of other AC resources in the microgrid in the extreme case of having a fault occurring simultaneously with a pulse load. It was also shown that the size of the supercapacitor can be reduced if the pulse load is temporary disconnected during the transient fault period. Simulations showed that the resulting supercapacitor size and the optimized controller parameters from the proposed two-level optimization scheme were feeding enough fault currents for different types of faults and minimizing the cost of the protection scheme.**

***Index Terms*— Adaptive protection, Optimization, Microgrid, Supercapacitor, Pulse load.**

I. INTRODUCTION

Microgrids are gaining increasing attention as an important part of the smart grid, due to their numerous benefits and their ability to operate both in islanded as well as in grid connected mode [1]. While such a diverse deployment of microgrids provide some important advantages, they pose some key challenges in terms of protection. A conventional protection system which is designed for passive distribution networks is no more suitable for the microgrids which are embedded in active distribution networks [2]. Moreover, high penetration of inverter interfaced generators in microgrids, significantly affects their short circuit capacity [3].

In order to protect AC microgrids in both grid-connected and islanded modes of operation, an adaptive protection scheme is required [4]. In [5]-[8], central protection approaches are proposed to calculate the fault current of the distributed energy resources (DERs). This system can be used to monitor a microgrid over communication lines and react to dynamic changes of the system. The authors in [9] change the time-current characteristics for short circuit and overload conditions by observing the difference in voltage drops during these two events respectively.

This work was partially supported by grants from the Department of Energy (DoE). The authors are with the Energy Systems Research Laboratory, Department of Electrical and Computer Engineering, Florida International University, Miami, FL 33174 (e-mail: mohammed@fiu.edu).

Nonetheless, a key disadvantage of the formal is the fact that these approaches are completely reliant on exchange or transfer of data/information in the shape of measured system parameters and direction and interlocking signals between different protection devices via some kind of communication link. The challenge is in the fact that in an extremely interconnected cyber-physical system, such as adaptive protection in microgrids, minor unconventionalities in the cyber domain can have catastrophic impacts in the physical domain [10].

Therefore, the goal of a resilient adaptive protection algorithm is to ride through communication failures without serious damage to hardware assets (transmission lines in this case), or financial losses.

Considering the above factors an adaptive protection scheme for AC microgrids, which is capable of surviving communication failures by the aid of supercapacitor, is a viable solution for enhancing the resiliency of adaptive protection to communication outages. In the normal case, the PCC senses microgrid's shift to islanded mode and thus issues a control command to the corresponding relays to shift their settings from high (which is between 6-7 times of the rated current value) to low (which is between 1.5-2.5 times of the rated current value). However, during communication outages, this process is not possible and thus relay settings remain high in islanded mode of operation.

Therefore in such situations, due to their fast responses, supercapacitor can be utilized to contribute to the fault current and raise this current value to a level which is sensed by the high relay settings. However, attention must be paid as not to oversize the utilized supercapacitor and therefore incur additional costs on the overall system. As such, this paper extends our previous work [11] by proposing a two-level optimization scheme for minimizing the supercapacitor size along with optimizing its controllers' parameters to reduce its fault current contribution and increase that of other AC resources in the microgrid. In order to ensure that the optimization process will converge to a sufficient supercapacitor size, this paper addresses the extreme case where a 3-phase to ground occurs during the period of a pulse load. The work in this paper also shows in a case study that the size of the supercapacitor can be reduced if the pulse load is temporary disconnected during the transient fault period. All simulated cases are investigated and showed that the optimization process did indeed reduce both the size and cost supercapacitor bank as well as maintain stable system operation.

The rest of the paper is organized as follows: Section II presents a system description. Section III details the proposed protection algorithm. Section IV discusses the supercapacitor's sizing process. Section V presents a discussion of the obtained results. Section VI presents the impact of reduced sizing of the cost of the supercapacitor bank. Finally, section VII concludes the paper.

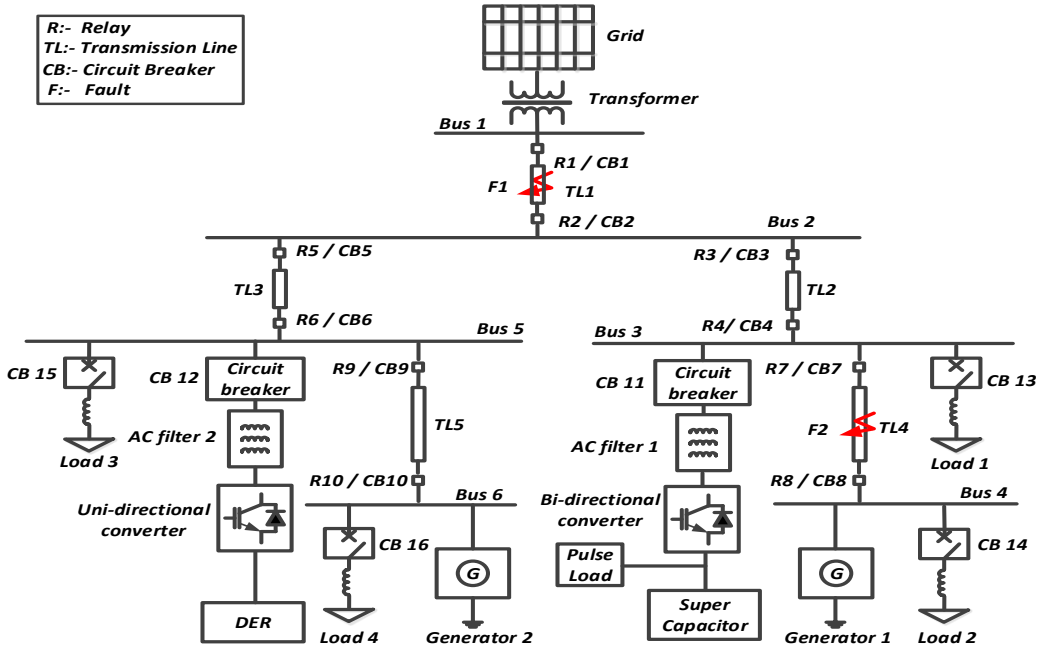

Fig.1. Configuration of the microgrid under study

II. HYBRID DC/AC MICROGRID DESCRIPTION

Fig.1 shows the topology of the hybrid DC/AC microgrid under study. The system has grid connection capabilities and contains two ac generators of 7.5 KVA, 60 HZ, 208 V and 1800 RPM synchronous machines coupled to individual induction motors as prime movers. A three phase 7.5 KVA Δ/Yg transformer is implemented to feed the AC microgrid with the required rated voltage. The system has a filter located between the transformer and the AC microgrid to filter out the harmonics of the AC grid with inductance of 4mH. Another AC filter is added between the AC and DC parts of the microgrid to improve the performance of the bidirectional and unidirectional converters and reduce the harmonics of the AC microgrid as well. The supercapacitor bank is 2.9F with rated voltage of 320V to feed a DC 12-Ω resistive pulse load. DER is also used to inject current to the AC side and help the generators feed different loads that are connected with circuit breakers at this side. The bidirectional converter that is connected between the supercapacitor and the AC side is used for charging the supercapacitor in the normal operation and the supercapacitor injects current to the AC side during fault condition in islanded mode of operation when the communication is not available. The unidirectional converter is present to allow DER to support AC sources in feeding various loads in the microgrid. A relay and a circuit breaker is connected to each end of all transmission lines. CB_{11} and CB_{12} are connected at the terminals of the DC sources and provide the ability to connect and disconnect these sources.

III. PROPOSED PROTECTION ALGORITHM

The logic algorithm of the relays during the different modes of operation under study, namely grid connected mode, islanded mode with communication, and islanded mode with loss of communication is shown in Fig. 2 and can be described in the following equations.

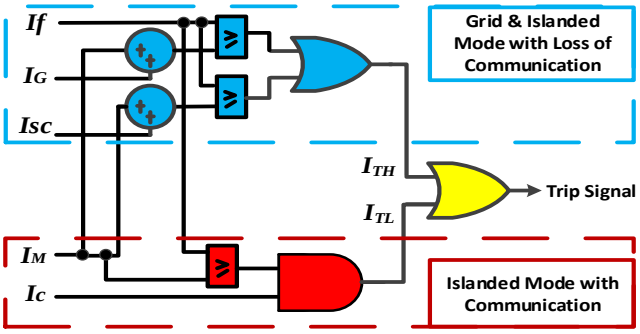

Fig.2 The Logic Diagram of the Relay.

Equation (1) gives the operation of the logic circuit of the relay at trigger high (I_{TH}) that represented high settings, when the system operates at grid connected or at islanded mode when the communication fails.

$$I_{TH} = \begin{cases} 1 & (I_f \geq I_G + I_M) + (I_f \geq I_{SC} + I_M) \\ 0 & otherwise \end{cases} \quad (1)$$

where I_f is the fault current, I_G, I_M and I_{SC} are the contribution currents from grid, microgrid and supercapacitor respectively.

Equation (2) describes the logic of the relay at islanded mode of operation when the communication is available in the system. In this case, the relay will produce (I_{TL}) and will be adjusted to low settings.

$$I_{TL} = \begin{cases} 1 & (I_f \geq I_m) \,.\, I_c \\ 0 & otherwise \end{cases} \quad (2)$$

where I_C is the communication signal issued from the PCC to the relay, adjusting its settings.

As indicated in equation (3), the relay will send a trip signal to the circuit breaker when either (I_{TH}) or (I_{TL}) is activated:

$$Trip\ signal = I_{TH} + I_{TL} \quad (3)$$

IV. THE SUPERCAPACITOR'S SIZING PROCESS

A two-level optimization process for proper sizing of the supercapacitor in the system under study is proposed, as shown in Fig .3. In Level 1, the main objective is to reduce the cost of the proposed protection scheme by selecting the value of the supercapacitor. In level 2, the main of objective of the optimization process is to minimize the supercapacitor's fault current contribution and maximize that of the distributed generators. This is achieved by optimizing the associated frequency, AC voltage, and DC voltage controllers. Fig. 4 shows the block diagram of the three PI controllers regulating the frequency, dc voltage and ac voltage of the system. As can be seen in Fig. 4, the error signals for the frequency and DC voltages (f_{er} and V_{dc_er}) are fed into the first and second PI controllers with parameters k_{p_f}, k_{i_f} and k_{p_vdc}, k_{i_vdc}, respectively.

These parameters are used to regulate the direct current component of the system (I_{d_r}), which in its turn regulates the frequency and DC voltage of the supercapacitor bank. Using the AC side frequency as a signature to the active power flow allows the supercapacitor to supply large currents during the fault and contribute to the fault current during loss of communication situations. The AC voltage error signal (V_{ac_er}) is given as input to the third PI controller with k_{p_vac} and k_{i_vac} parameters that used to regulate the quadratic current component of the system (I_{q_r}), and regulates the AC voltage.

Based on the inverse Park transformation the reference three phase currents (I_{a_r}, I_{b_r}, and I_{c_r}) are estimated from the dq0 rotating reference frame currents. The angle between the two reference frames and the system frequency are estimated from three-phase Phase Locked Loop block (PLL).

The abc reference currents are compared with the actual measured currents and applied to the pulse width modulation (PWM) scheme to generate the switching signals of the inverter. The hysteresis band current control is considered in this work because of its simplicity of implementation and fast response current loop. It also doesn't need any knowledge of the load parameters.

The proposed algorithm is an iterative one, which is also combined with a Particle Swarm Optimization (PSO) routine. On the first level, the process first starts by selecting a set of possible values of capacitances, C_i's, such that $C_{min} < C_i < C_{max}$, based on physical constraints of the microgrid under study. A predefined $\Delta C = 0.2\,F$ was selected in our analysis. It's worth noting that selecting ΔC requires a tradeoff between the optimizations accuracy and the processing time. It was found that $\Delta C = 0.2\,F$ was an adequate value that preserves the optimization's accuracy and does not incur excessive processing time. On the second level, for every capacitance value, C_i the PSO routine is started in order to optimize the associated frequency, AC, and DC voltage controllers.

As mentioned earlier, the controllers in this work are PI controllers, and thus, the parameters to be optimized are the $K_p's$ and $K_i's$ for each controller. For the PSO routine, a search space is randomly generated by defining a population of varying combinations of candidate $K_p's$ and $K_i's$ for the aforementioned controllers. In order to evaluate the fitness function, the PSO routine was interfaced with a Simulink model of the power microgrid with its controllers to evaluate their response to the different particles in the generated swarm and thus retrieve the capacitor's current fault contribution.

The population generation process is bounded by a vector of lower bounds (LB) and upper bounds (UB) for each controller. Proper definition of the lower and upper bounds is imperative for the success of the optimization process.

Table I, shows the search space for the parameters to be optimized. During the entire simulation, the solution of the optimization processes is bounded by constraints on the system frequency, AC voltage, and DC voltage in order to ensure stable operation of the microgrid.

In fact, two set of constraints were imposed: one during steady state (ss) operation and the other during the pulse load and fault condition, where the accepted limits for these constraints are not the same at normal and abnormal conditions as indicated in equations (4-9).

$$f_{min1} < f_{ss} < f_{max1} \tag{4}$$

$$f_{min2} < f_{fault} < f_{max12} \tag{5}$$

$$Vac_{min1} < Vac_{ss} < Vac_{max1} \tag{6}$$

$$Vac_{min2} < Vac_{fault} < Vac_{max2} \tag{7}$$

$$Vdc_{min1} < Vdc_{ss} < Vdc_{max1} \tag{8}$$

$$Vdc_{min2} < Vdc_{fault} < Vdc_{max2} \tag{9}$$

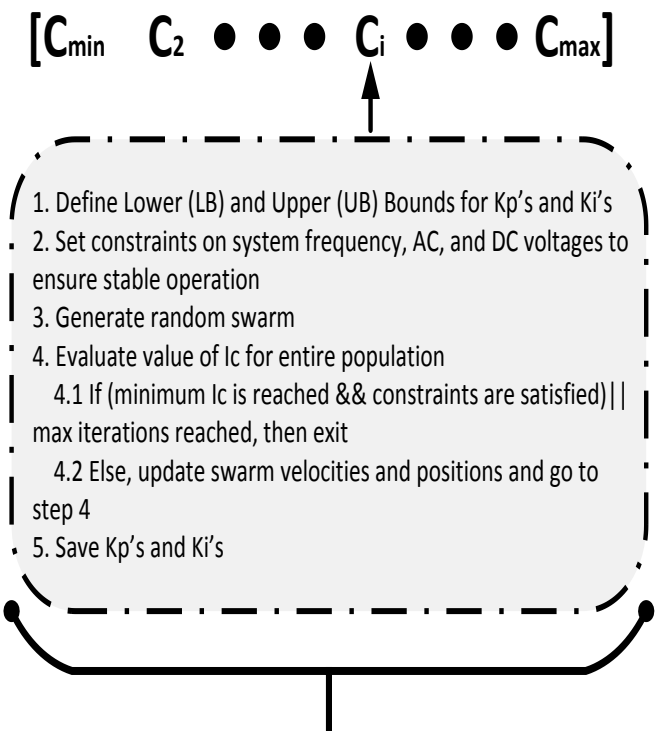

Fig. 3. The Combined iterative optimization process for supercapacitor sizing

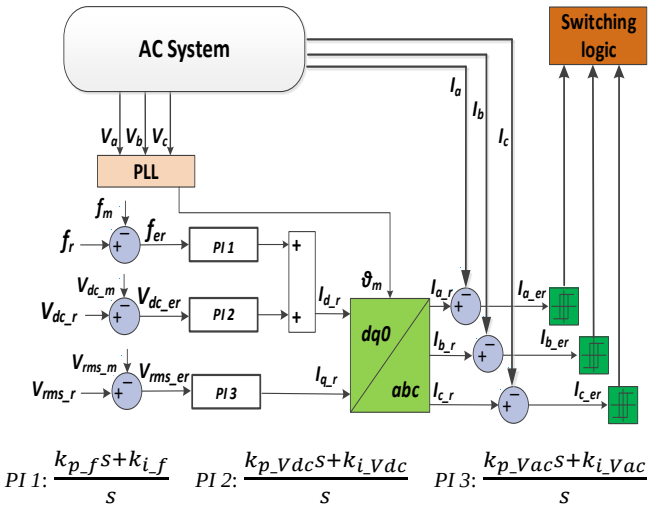

$PI\ 1: \frac{k_{p\_f}s+k_{i\_f}}{s}$ $PI\ 2: \frac{k_{p\_Vdc}s+k_{i\_Vdc}}{s}$ $PI\ 3: \frac{k_{p\_Vac}s+k_{i\_Vac}}{s}$

Fig. 4. Converter control logic block diagram

Table I. Lower and Upper Bounds of Optimization Variables

Parameter	Lower Limit	Upper Limit
C	1.5	2.7
Frequency K_p	10	80
Frequency K_i	80	140
AC Voltage K_p	10	50
AC Voltage K_i	100	150
DC Voltage K_p	10	40
DC Voltage K_i	80	160

V. Results and Discussion

In this section, multiple case studies were performed in order to investigate the performance of the proposed supercapacitor sizing algorithm. The system was first simulated in islanded mode without communication during the extreme case of having a three phase to ground fault during a pulse load peak period. Next, the system was simulated under the same conditions but using the optimized controller parameters that limits the supercapacitors fault current contribution and the obtained supercapacitor size. Finally, the case where the pulse load was temporarily disconnected from the system during the transient fault period was investigated. The supercapacitor's fault current contribution along with the overall system stability was recorded and analyzed in what follows.

Case I: Islanded Mode of Operation without Communication and During Supercapacitor Discharging Period

A three-phase to ground fault (F_1 in Fig. 1) has been applied in the transmission line (TL_1) at time t=1.5 seconds, while the microgrid was in grid connected mode of operation. As a result relay R_1 will send a trip signal to circuit breaker CB_1 to isolate the microgrid. The microgrid successfully shifted to a stable islanded mode by adjusting its overall frequency back to the normal condition after the fault, as shown in Fig. 5(a). A small disturbance, within acceptable limits, in the output voltages of the sources (V_G, V_{g1}, V_{g2}, V_{inv1} and V_{inv2} representing the voltages at busses 1, 4, 6, 3 and 5, respectively), is noticed in Fig. 5(b). Fig. 5(c) and (d) show the supercapacitor-pulse load microgrid

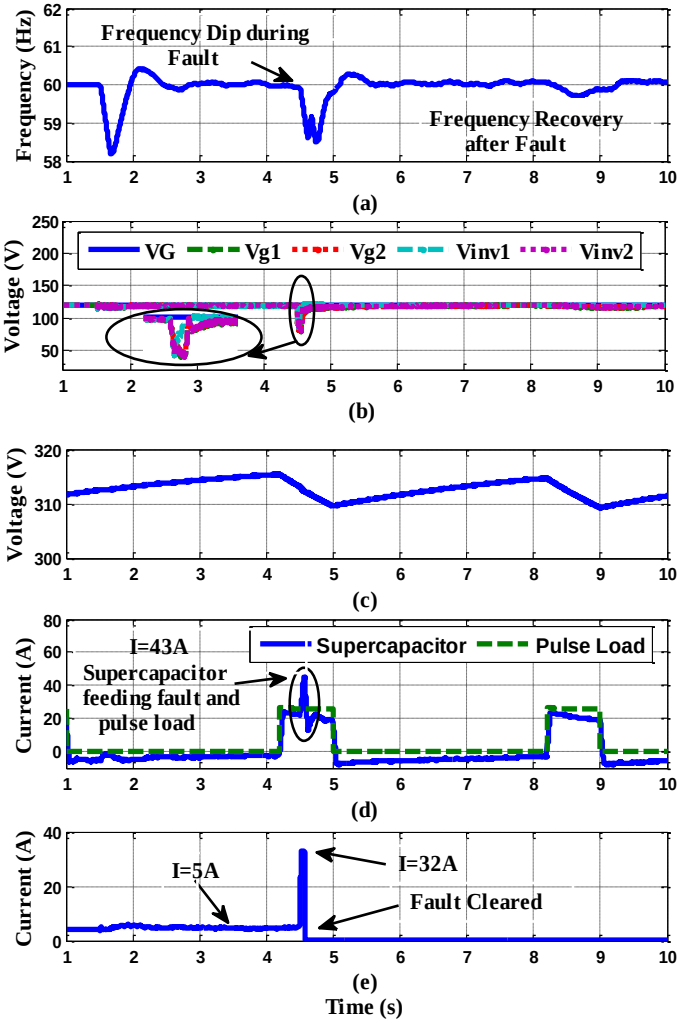

Fig. 5. System performance during fault at microgrid operation without communication (a) frequency, (b) output voltage of each source, (c) supercapacitor DC voltage, (d) supercapacitor current, and pulse load current, (e) RMS current in the faulted transmission line TL4.

performance parameters which exhibit stable performance during the islanding instant. Finally, Fig. 5(e) indicate the minor change in the AC current at transmission line TL_4 after the fault. During the islanded operation, another three-phase-to-ground fault occurred at t = 6 seconds during the on-time of the pulse load (i.e. discharging of the supercapacitor) in the middle of transmission line (TL_4). Due to the assumption of the communication failure, relay R_7 will not be able to switch to the lower settings and the supercapacitor quickly contributed to the fault current while still covering the pulse load. Fig 5(a) shows the microgrid frequency recovery after the fault incident. As can be noticed the system is showing stable performance during and after the fault with disturbances within the specified limits of microgrids operation. The sources voltages V_{g2}, V_{inv1} and V_{inv2} dropped at the fault incident and recovered after clearing the fault, as shown in Fig. 5(b). As indicated in Fig. 5(d), the maximum current drawn from the supercapacitor in this case is 43 Amps which is required to feed the fault and the pulse load simultaneously. Fig. 5(e) shows that the fault current drastically increased from 5 Amps to 32 Amps. This resulted in relay R_7 sensing the fault and sending trip signal to CB_7 to isolate the fault.

Case II: System Performance with Optimized Supercapacitor Size

In this case, the optimized frequency, AC, and DC voltages controllers were utilized along with the obtained supercapacitor size of 2.5F (compared with the original 2.9F). Fig. 6(a) shows a stable system performance, with the new parameters, in terms of its frequency during the first fault to isolate the microgrid as well as during the second fault. It can be noted that the drop of frequency during the second fault is less than the drop without optimized parameters. Fig. 6(b) shows that the drop in the sources' voltages (V_G, V_{g1}, V_{g2}, V_{inv1} and V_{inv2}) is within accepted limits during both faults. Fig. 6(d) shows that the amount of current that was injected by the supercapacitor is reduced to 38 Amps compared to 43 Amps in the previous case. This plays a major role in reducing the size of the supercapacitor and thus it's cost as it will be shown in the next section. Fig. 6(e) shows that the relay reached its high setting value as a result of increasing the amount of current from the AC side even during communication outages.

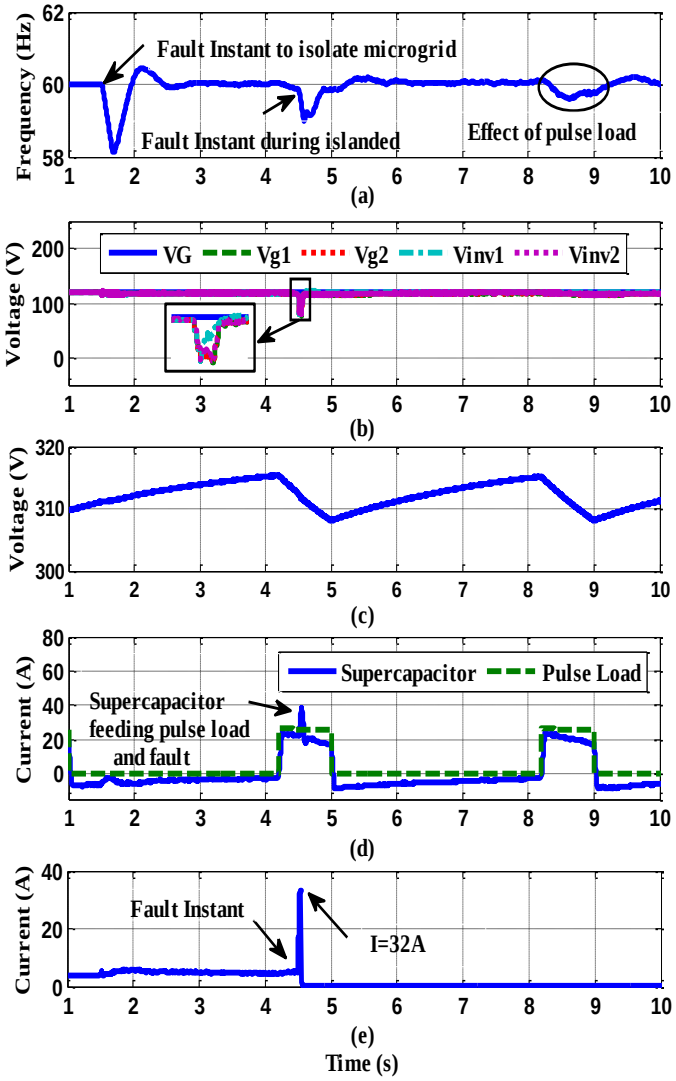

Fig. 6. System performance during fault at microgrid operation without communication with optimized supercapacitor size (a) frequency, (b) output voltage of each source, (c) supercapacitor DC voltage, (d) supercapacitor current, and pulse load current, (e) RMS current in the faulted transmission line TL4.

Case III: Disconnecting the Pulse Load During the Fault Period

Similar to the previous case, fault F_2 occurred during the on-time period of the pulse load. It is noticed in Fig. 7(a) that, due to communication failure, relay R_7 will not switch to the lower settings and the supercapacitor quickly contributed to the fault current. However, in this case, the pulse load was disconnected for a short period of time during the fault in order to reduce the amount of current drawn from the supercapacitor which reached a maximum of 27 Amps in this case. To disconnect the pulse load, the rate of change of the supercapacitor's voltage was monitored to detect a small notch in the DC voltage indicating the fault as shown in Fig. 7(b) and (c).

Table. II shows the operation of the system under different types of faults for the initial supercapacitor value of 2.9F and the optimized value 2.5F. For three phase to ground fault with fault resistance 2-Ω, it can be noted that at grid connected mode, the fault current reach to 32 Amps that is more than 6 times the rated current which is 5 Amps. For islanded mode of operation, when the communication is available and the relays can adjust its settings from grid mode (6-7 times rated current) to the islanded mode (1.5-2.5 times rated current), the relay can send a trip signal to the circuit breaker and isolate the fault. During islanded mode without communication case, the maximum current drawn from the supercapacitor for the initial case with rating 2.9F is 43 Amps which is required to feed the fault and the pulse load simultaneously. Thus, the optimized supercapacitor and controller's values can compensate the amount of current that is required to reach to the setting of the relay during discharging the supercapacitor and feed the pulse load with I_C=38 Amps. This current is less than the initial supercapacitor case (43 Amps) by 5 Amps, while the contribution from AC microgrid increased to 18 Amps instead of 14 Amps in order to reach to the relay setting.

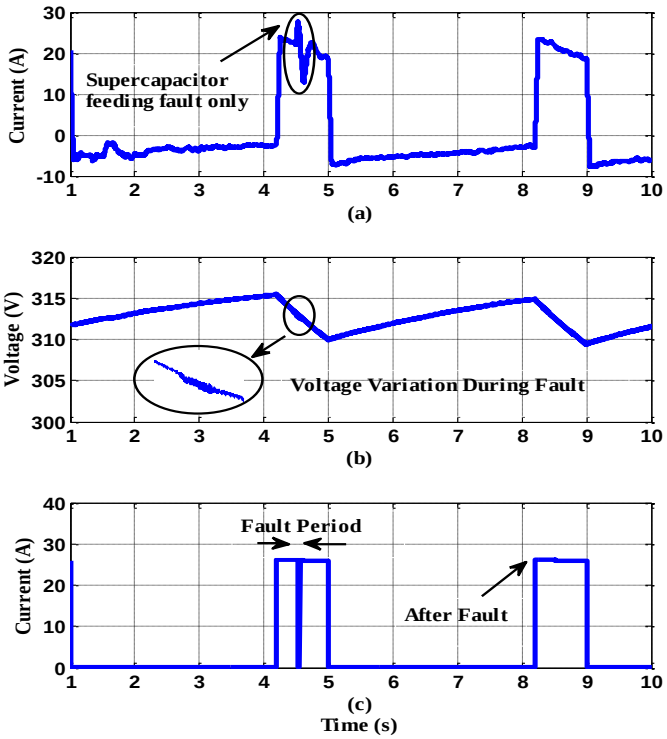

Fig. 7. System performance during fault at microgrid operation without communication (a) supercapacitor current, (b) supercapacitor DC voltage, (c) pulse load current.

Table II. Different types of faults with the rating of Supercapacitor with and without optimization

Fault Type	R_f (Ω)	Relay Setting During Grid Mode (A)	Relay Setting During Islanded mode with Communication (A)	Islanded mode without Communication During Discharging Supercapacitor at Case I				Islanded mode without Communication During Discharging Supercapacitor at Case II			
				Ic	Im	Ipl	RS	Ic	Im	Ipl	RS
ABCG	2	32	12	43	12	23	32	38	18	23	32
BCG	1.8	30	10	41	15	23	30	33	20	23	30
AG	0.1	18	8	23	18	23	18	23	18	23	18

R_f = Fault Resistance; RS = Relay Settings; I_C = Supercapacitor current contribution; ; I_m = Microgrid current contribution; ; I_{PL} = Current drawn from supercapacitor to feed the pulse load

Similarly, in the case of a double-line-to-ground fault (BCG), the initial supercapacitor and the optimized supercapacitor and controller's values can be sufficient to compensate the amount of current that needed between grid and islanded modes.

Finally, the AC microgrid generating units were capable of feeing sufficient fault current for fault detection in the case of a single-line-to-ground fault without the need of supercapacitor that can be used to feed only pulse load in this case.

VI. IMPACT OF REDUCED SIZING OF THE COST OF THE SUPERCAPACITOR BANK

During energy utilization of a supercapacitor bank, its terminal voltage will vary with time. So, the total energy (E_1) that can be delivered by the supercapacitor can be expressed by:

$$E_1 = \frac{1}{2}(V_{max} - V_{\min})^2 \qquad (10)$$

Where V_{max} is the maximum voltage of a supercapacitor bank during a pulse load and V_{min} is its minimum voltage. In the proposed hybrid DC microgrid, the maximum acceptable variation of the DC bus voltage is limited to $\pm 5\%$.

In order to evaluate the economic benefits of the proposed optimization method, a financial estimation of the supercapacitor cost is performed. The commercial price of the supercapacitor Model BMOD0058-E016-B02 manufactured by Maxwell [12], is 122.25$.

Table. III shows the optimization results of the cost of the supercapacitor bank, where E_2 is the stored energy per module, (E_1/E_2) represents the approximate number of required modules.

It can be noted from the table that the sizing and cost of supercapacitor bank is reduced from 2.9F to 2.5F and the total cost is reduced from 12155.14$ to 10478.57$ as a result of the optimization process.

Also, in the case where pulse load was temporarily disconnected during the fault, the supercapacitor's cost was reduced by 12155.14$ to 6339.53$.

Henceforth, the proposed sizing algorithm along with optimizing the corresponding controller parameters is suitable feasible and produced excellent results. It is shown that the size and cost of the supercapacitor were minimized, while the system is still meeting the protection and safe operation requirements.

This is very beneficial when the system has pulsed loads as these types of loads do not tolerate any interruption during their turned on period.

It is important to mention here, that the other proposed solution of temporarily disconnecting the pulse load is suitable for noncritical pulse loads.

Table III. Cost estimation of the supercapacitor bank.

C	V_{max}	V_{min}	E1	E2	E1/E2	Price
2.9	322	310	208.8	2.1	99.42	12155.14
2.5	321	309	180	2.1	85.71	10478.57
1.8	320	309	108.9	2.1	51.85	6339.53

VII. CONCLUSION

This paper proposes two solutions for reducing the size and cost of supercapacitors that are used to compensate for the islanded microgrid fault currents during communication outages in adaptive protection schemes. First, for critical pulse loads, a two-level optimization is presented. The resulting reduced size of the supercapacitor is investigated under several types of faults and the simulation results shows the ability of the new supercapacitor rating to feed different types of faults. Second, temporary disconnection of pulsed load during the transient fault period proved effective for non-critical pulse loads as a solution to avoid utilization of oversized supercapacitors.

REFERENCE

[1] J. Tang, Y. Gong, N. Schulz, M. Steurer and P. G. McLaren, "Implementation of a Ship-Wide Area Differential Protection Scheme," in *IEEE Transactions on Industry Applications*, vol. 44, no. 6, pp. 1864-1871, Nov.-Dec. 2008.

[2] O. V. Gnana Swathika and S. Hemamalini, "Prims-Aided Dijkstra Algorithm for Adaptive Protection in Microgrids," in *IEEE Journal of Emerging and Selected Topics in Power Electronics*, vol. 4, no. 4, pp. 1279-1286, Dec. 2016.

[3] Hany F. Habib; T. Yossef; O. Mohammed, "A Multi-Agent Based Technique for Fault Location, Isolation, and Service Restoration," in *IEEE Transactions on Industry Applications* , vol. no.99, pp.1-1, Feb. 2017.

[4] Ustun, T.S.; Ozansoy, C.; Zayegh, A., "Modeling of a Centralized Microgrid Protection System and Distributed Energy Resources According to IEC 61850-7-420," in *IEEE Transactions on Power Systems*, vol.27, no.3, pp.1560,1567, Aug. 2012.

[5] Laaksonen, H.J., "Protection Principles for Future Microgrids", in *IEEE Trans. Power Electronics*, vol.25, no.12, pp.2910,2918, Dec. 2010.

[6] Najy, W.K.A; Zeineldin, H.H., "Optimal Protection Coordination for Microgrids With Grid Connected and Islanded Capability,", in *IEEE Trans, Industrial Electronics* , vol.60, no.4, pp.1668,1677, April 2013.

[7] Laaksonen, H.; Ishchenko, D.; Oudalov, A, "*Adaptive Protection and Microgrid Control Design for Hailuoto Island*", in *IEEE Trans. On Smart Grid*, vol.5, no.3, pp.1486,1493, May 2014.

[8] T. S. Ustun, C. Ozansoy, A. Zayegh, "Modeling and simulation of a microgrid protection system with central protection unit", in *IEEE TENCON Spring Conference*, pp. 5-9, 2013.

[9] R.M. Tumilty, M. Brucolit, G.M. Burt and T.C. Greent , " Approaches to Network Protection for Inverter Dominated Electrical Distribution Systems', in *the 3rd IET, Machines and Drives*, pp. 622-626, 2006.

[10] R. Akella, H. Tang, and M.M. Bruce, "Analysis of Information Flow Security in Cyber-Physical System", in *International Journal of Critical Infrastructure Protection*, Vol. 3, pp: 157-173, 2010.

[11] Hany. F. Habib, A. A. S. Mohamed, Mohamad. El Hariri and Osama. A. Mohammed, "Utilizing Supercapacitors for Resiliency Enhancements and Adaptive Microgrid Protection against Communication Failures", in *Electric power systems Research*, vol.145, pp.223-233, Apr., 2017.

[12] Maxwell, 16V small cell module, Model: BMOD0058 E016 B02 (16.2V-58 F), San Diego, CA. Available Online at: http://www.maxwell.com/images/documents/datasheet_16v_small_cell_module.pdf.